HOKKAIDO UNIVERSITY

Title	The Irradiation Effect of a Simultaneous Laser and Electron Dual-beam on Void Formation
Author(s)	Yang, Zhanbing; Watanabe, Seiichi; Kato, Takahiko
Citation	Scientific Reports, 3, 1201 https://doi.org/10.1038/srep01201
Issue Date	2013-02-04
Doc URL	http://hdl.handle.net/2115/51914
Rights(URL)	http://creativecommons.org/licenses/by-nc-nd/3.0/
Type	article
File Information	srep01201.pdf

Instructions for use

Hokkaido University Collection of Scholarly and Academic Papers : HUSCAP

SCIENTIFIC REPORTS

OPEN

SUBJECT AREAS:
MATERIALS SCIENCE
ENGINEERING
APPLIED PHYSICS
NUCLEAR PHYSICS

Received
23 July 2012

Accepted
16 January 2013

Published
4 February 2013

Correspondence and requests for materials should be addressed to S.W. (sw004@eng.hokudai.ac.jp)

The Irradiation Effect of a Simultaneous Laser and Electron Dual-beam on Void Formation

Zhanbing Yang[1], Seiichi Watanabe[1] & Takahiko Kato[2]

[1]Centre for Advanced Research of Energy and Materials, Faculty of Engineering, Hokkaido University, N13, W8, Kita-ku, Sapporo, Hokkaido 060-8628, Japan, [2]Hitachi Research Laboratory, Hitachi, Ltd., 7-1-1 Omika, Hitachi, Ibaraki, 319-1292, Japan.

Randomly distributed lattice point defects such as supersaturated vacancies (SVs) and Frenkel-pairs (FPs, an interstitial and a vacancy) can be simultaneously introduced into the crystal by energetic beam irradiation in outer space and/or nuclear reactors, but their behavior has not been fully understood. Using a high-voltage electron microscope equipped with a laser (laser-HVEM), we show the striking effects of simultaneous laser-electron (photon-electron) dual-beam irradiation on void formation. Our results reveal that during laser-electron sequential irradiation, pre-laser irradiation enhanced void nucleation and subsequent electron irradiation enhanced void growth. However, the laser-electron dual-beam irradiation was analyzed to depress void swelling remarkably because the recombination of SVs and interstitials was enhanced. The results provide insight into the mechanism underlying the dual-beam radiation-induced depression of void swelling in solids.

Material simulations of high-energy radiation environments, such as those existing in outer space[1] and inside nuclear reactors[2], are usually performed experimentally[3] and theoretically[4] to investigate the behaviour of lattice point defects, i.e. vacancies and interstitials[5,6]. These primary defects govern not only material microstructural changes, such as the formation of dislocation loops and voids[7–9], but also material mechanical property changes[10], for example embrittlement[11], creep[12] and hardening[13]. Although simulation studies have been performed for decades, reports of microstructural changes caused by the simultaneous presence of SVs and FPs are limited, except under ion-electron dual-beam irradiation[14]. Here we show the striking effects of simultaneous irradiation with a laser-electron (photon-electron) dual-beam on void formation in an *in situ* experiment using a laser-HVEM[15,16]. The laser-HVEM simultaneously introduces SVs and FPs into crystalline solids, as a result of the high intensity photon irradiation from the laser source and the electron irradiation from the HVEM[16], respectively.

Void formation and swelling introduced by irradiation have attracted considerable attention since their discovery in SUS316 steels in 1960[7,17–19]. SVs and interstitials simultaneously form in materials exposed to outer space or the inside of nuclear reactors through irradiations (neutron, heavy ion, γ-ray and electron), but experimental simulations of this condition have not been accomplished because of the technical limitations associated with nano-scale *in situ* observations. The use of *in situ* observation to realise this simulation is essential to understanding void formation and swelling in the outer space or the inside of nuclear reactors.

Since the first report in 1960[20], laser technology has been widely applied in various fields, such as surgery[21], radar[22], welding[23], material surface modification[24] and semiconductor material science[25]. As a result of their affordability, laser heads can be combined with other equipment to investigate new methods for exploring unknown scientific fields, such as the newly developed laser-HVEM used for materials studies[15]. The primary advantages of laser-HVEM can be summarised as follows. First, *in situ* observations of the evolution of material microstructures under laser irradiation are possible[16]. This method can directly record the evolution procedure and may also reveal the driving mechanism. Second, the evolution of defect structures under laser irradiation provides new measurements for defect migration energy[16] as a function of annealing temperature and time. These measurements have led to new lattice defect studies after little activity in the field for more than 30 years. Third, by precisely controlling the laser intensity and the electron dose rate, a laser-HVEM makes it possible to introduce randomly distributed SVs and FPs simultaneously into a crystalline solid. This approach is different from electron irradiation and cascade irradiation (neutron or heavy ions). During electron irradiation, only FPs are introduced, and no cascade damage results[26]. In the cascade irradiation process, the primary results of the cascade damage are

high concentrations of vacancies surrounded by interstitials[27]. Using a laser-HVEM, *in situ* observations of lattice defects under a photon-electron dual-beam irradiation process, which have never been reported to date, are possible.

SUS316L austenitic stainless steel is generally used for core-internals in boiling water reactors; in this study, SUS316L austenite steel was experimentally investigated to determine the effect of laser-electron dual-beam irradiation on void formation and swelling. The results were compared to those for steel subjected to laser-electron sequential irradiation and electron irradiation. Defect rate equations from various irradiation processes were proposed for a theoretical analysis of lattice point defect behaviours. We anticipate not only that the results will provide insight into the mechanism underlying the dual-beam radiation-induced depression of void swelling in solids but also that laser-HVEM will be employed for broader materials research in the future, such as simulation of the environment of outer space, laser-assistant welding and laser fabrication.

Results

Figure 1(a), (b), (c), (d) and (e) shows that void formation differs significantly under various irradiation conditions as mentioned in Table 1. For example, under electron (e^-) irradiation (Fig. 1(a)) and laser-electron ($L \rightarrow e^-$) sequential irradiation (Fig. 1(c) and (d)), a large number of voids are clearly observed; only a few very small voids form under laser irradiation, as the magnified image shows in Fig. 1(b); Fig. 1 (e) shows that under laser-electron simultaneous dual-beam ($L+e^-$) irradiation, void size seems smaller than that of e^- irradiation. Individual diagrams of the irradiation procedure are provided under each image to better illustrate the process. Statistical results for the void mean size, number density and swelling are shown in Fig. 2(a), (b) and (c), respectively.

The voids formed under e^- irradiation alone were found to have a mean size of 21.8 nm and a number density of 1.4×10^{20} m^{-3}. Under laser irradiation, voids still formed but were found to have the smallest mean size (4.4 nm) and lowest number density (0.7×10^{20} m^{-3}) among the different irradiation methods investigated. Under $L \rightarrow e^-$ irradiation, the voids were found to be much larger than the voids formed using laser irradiation alone, and the void number densities were much higher than those observed for e^- irradiation alone. This result indicates that pre-laser irradiation enhances void nucleation, and subsequent electron irradiation enhances void growth under the present experimental conditions. The mean void size for $L+e^-$ irradiation is smaller than that of e^- irradiation and $L \rightarrow e^-$ irradiation. However, the void number density is still much higher than that of e^- irradiation.

Statistical results of void swelling representing the comprehensive results of void mean size and number density are shown in Fig. 2(c). It is clear that under $L \rightarrow e^-$ irradiation, the void swelling is much greater than that with e^- irradiation, suggesting that $L \rightarrow e^-$ irradiation enhances void swelling. In the case of $L+e^-$ irradiation, void swelling was only 15% and 10%, respectively, of that observed for e^- irradiation and $L \rightarrow e^-$ irradiation. This illustrates the striking phenomena of $(L+e^-) < e^- < (L \rightarrow e^-)$ regarding void swelling.

Discussion

A theoretical explanation of defect behaviour during e^- irradiation has been proposed by Kiritani *et al.*[28]and by Sizmann[29]. FPs are introduced during e^- irradiation, and equations for the concentra-

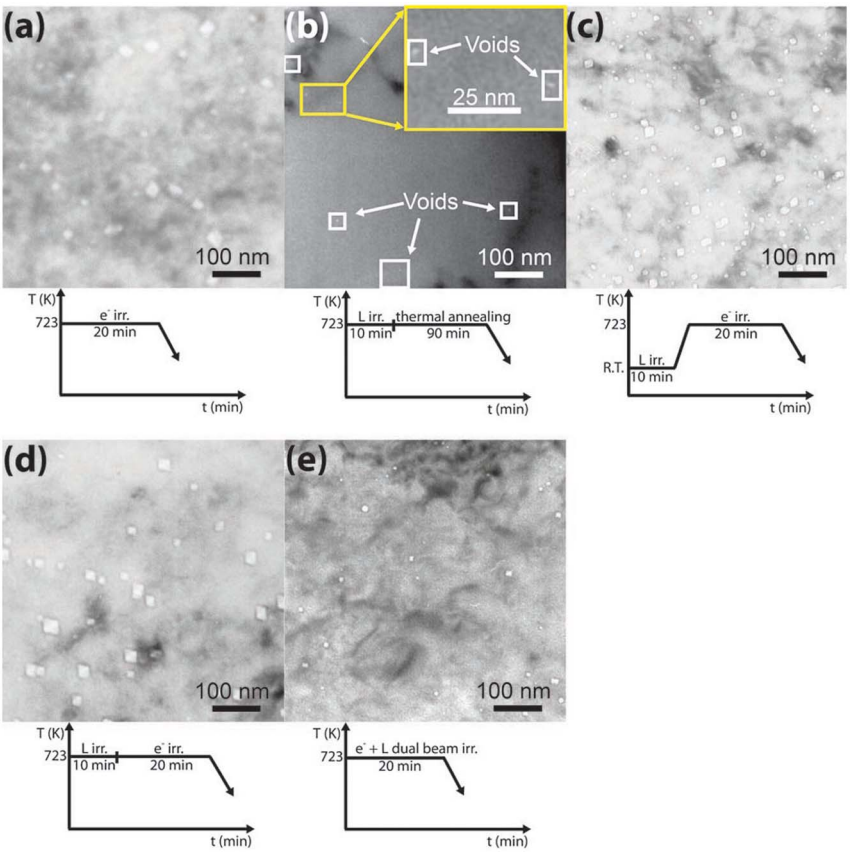

Figure 1 | Void formation in SUS316 under the five different irradiation conditions. (a) Electron irradiation at 723 K for 20 min. (b) Laser irradiation at 723 K for 10 min followed by thermal annealing at 723 K for 90 min. (c) Laser irradiation at R.T. for 10 min followed by electron irradiation at 723 K for 20 min. (d) Laser irradiation at 723 K for 10 min followed by electron irradiation at 723 K for 20 min. (e) Simultaneous laser and electron dual-beam irradiation at 723 K for 20 min.

Table 1 | Details of the five experimental irradiation procedures

Number	Experimental Procedure
Irr. 1	Electron irradiation at 723 K for 20 min. (e^-)
Irr. 2	Laser irradiation at 723 K for 10 min (1200 pulses) followed by thermal annealing at 723 K for 90 min. (L)
Irr. 3	Laser irradiation at R.T. for 10 min (1200 pulses) followed by electron irradiation at 723 K for 20 min. (L (R. T.)→e^-)
Irr. 4	Laser irradiation at 723 K for 10 min (1200 pulses) followed by electron irradiation at 723 K for 20 min. (L (723 K)→e^-)
Irr. 5	Laser-electron simultaneous dual-beam irradiation at 723 K for 20 min. (L+e^-)

tion variation of the vacancies C_v and the interstitials C_I are given as follows:

$$\frac{dC_V}{dt} = K - R_{IV}(D_I + D_V)C_I C_V - S_V D_V C_V, \quad (1)$$

$$\frac{dC_I}{dt} = K - R_{IV}(D_I + D_V)C_I C_V - S_I D_I C_I, \quad (2)$$

where K is the point defect production rate under e^- irradiation, R_{IV} is the capture site number of the recombination of the interstitials and vacancies, S_V and S_I are the sink strengths of the vacancies and interstitials, respectively, and D_V and S_I are the diffusivities of the vacancies and interstitials, respectively. The time dependences of C_v and C_I are shown in Fig. 3(a). The dark line represents e^- irradiation with $S = 2 \times 10^{14}$ m^{-2} which is a general magnitude under e^- irradiation. Because FPs are introduced by e^- irradiation, C_v and C_I continuously increase until the vacancies and interstitials begin to recombine at t_1. During the $t_2 - t_3$ period, C_I begins to decrease because of the sink, which contributes to the annihilation of the interstitials, whereas C_v increases because of the lower mobility of the vacancies. A steady-state region occurs at t_3; at this point, the defects have equivalent annihilation rates because the sink starts to contribute to vacancy annihilation.

For laser irradiation, after introduced at the surface of the specimen, all SVs diffuse to the interior and distribute homogeneously inside the specimen[16]. Thus, C_v is rewritten as:

$$\frac{dC_V}{dt} = L - S_V D_V C_V, \quad (3)$$

where L is the SV production rate under laser irradiation. The recombination term is ignored because no interstitials exist. The time dependence of C_v is shown in Fig. 3 (b). Even after a subsequent thermal annealing period of 90 min, SVs prefer to form vacancy-type loops[16]. The SVs appear to be "frozen" and do not contribute to void growth; but might actually nucleate the invisible void nuclei and vacancy-type clusters.

In the case of L→e^- irradiation, during pre-laser irradiation, C_v can be given by eq. (3) and is illustrated in Fig. 3 (c) by a red dot line. During subsequent electron irradiation, C_v and C_I can be expressed as:

$$\frac{dC_V}{dt} = K - R_{IV}(D_I + D_V)C_I C_V - S_V D_V C_V, \quad (4)$$

$$\frac{dC_I}{dt} = K - R_{IV}(D_I + D_V)C_I C_V - S_I D_I C_I, \quad (5)$$

the time dependences of C_v and C_I are shown in Fig. 3(c). t′ is the time from 600 s which is the starting point of subsequent electron irradiation. At the initial stage of subsequent electron irradiation, interstitials firstly annihilate to SVs introduced by pre-laser irradiation, once an interstitial leaves its position from a FP to recombine with a SV, the remaining vacancy becomes a new SV. After

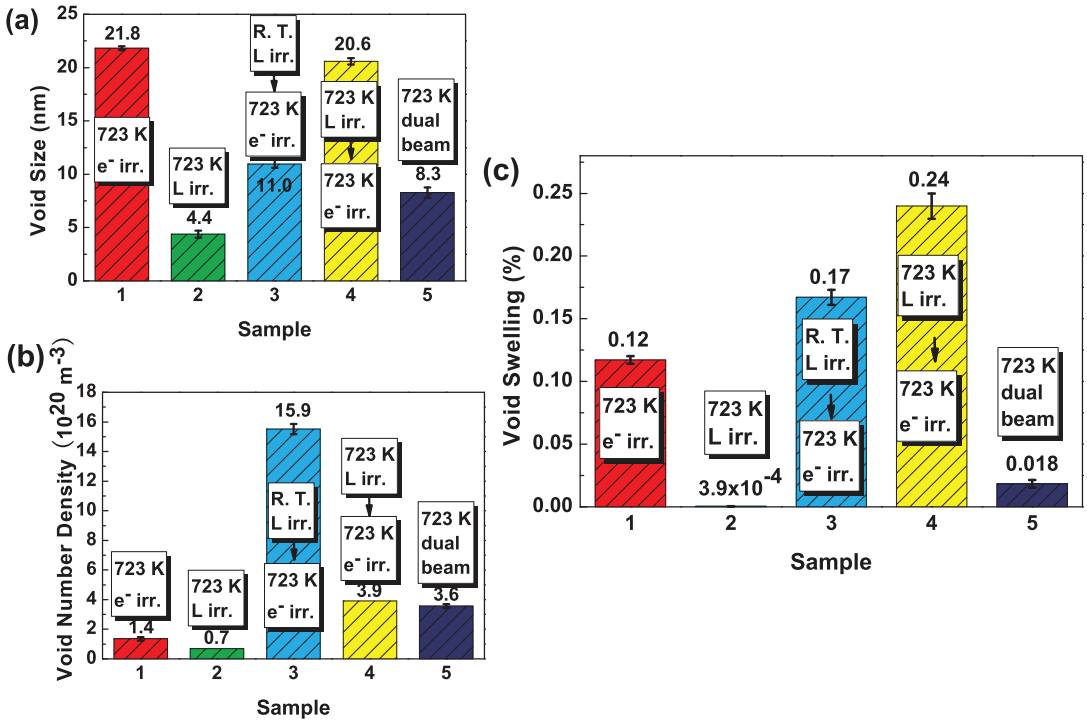

Figure 2 | Statistical results for the void size (a), number density (b) and swelling (c) of the specimen under five different irradiation conditions. The error bars represent the standard deviation.

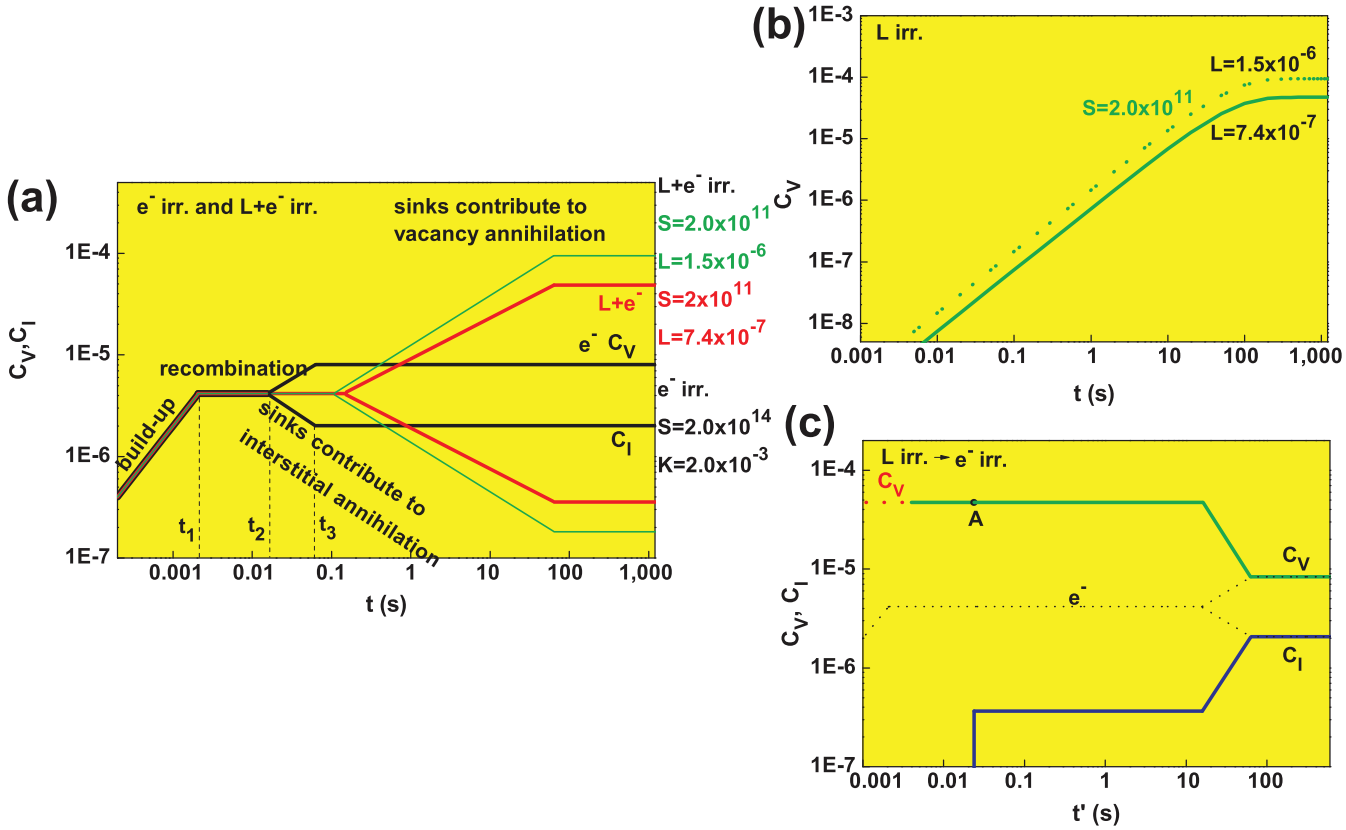

Figure 3 | Calculated time dependences of C_V and C_I under different irradiation conditions. (a) Electron irradiation and laser-electron dual-beam irradiation for 20 min. (b) Laser irradiation for 10 min. The SV production rate increases with laser intensity, as the dot line shows. (c) Laser irradiation for 10 min followed by electron irradiation.

the annihilation, interstitials enter a very quick build-up stage; accordingly, C_v also increases. Because the increment is relative much smaller, the build-up stage of C_v is marked as the dark dot A in the line. Compared with the e^- irradiation (without pre-laser irradiation, as shown in Fig. 3(c) by the dark dot line), it is obvious that before the steady-state C_v of L→e^- irradiation is higher than that of e^- irradiation. Consequently, void number density of L→e^- irradiation is higher than that of e^- irradiation. By eqs. (4) and (5), L→e^- irradiation finally reaches to the same steady state with e^- irradiation; different from the e^- irradiation, during L→e^- irradiation C_v does not increase but decrease after the recombination stage by the SVs' diffusion to sinks because of the high C_v. Voids grow during the entire procedure and therefore are much larger than those observed for e^- irradiation. From this finding, it becomes obvious that subsequent electron irradiation enhances void growth, which begins as the electron irradiation perturbs the "frozen" SVs. This mechanism can be explained as follows. During pre-laser irradiation, SVs form stable invisible vacancy-type clusters and void nuclei; the subsequent electron irradiation enhances the SVs migration, thus the "frozen" SVs become movable and contributive to void growth.

One experimental difference between the two types of L→e^- irradiation (denoted as Irr. 3 and Irr. 4 in Table 1) is the temperature of the laser used for irradiation. SVs are stable at R.T. but are mobile during the heating procedure from R.T. to 723 K. As a result, new voids nucleate, and these differ from those that become nucleated during pre-laser irradiation. This causes the void number density of Irr. 3 to be higher than that of Irr. 4. Both subsequent electron irradiation processes were carried out at 723 K for 20 min, with the same damage rate being observed for each. Stated another way, the effect of subsequent electron irradiation on perturbing the "frozen" vacancies for void growth is the same. If it is assumed that the growth of void nuclei is homogeneous, the void mean size of Irr. 3 should be smaller than that of Irr. 4 due to the higher void number density of Irr.3.

In the case of dual-beam irradiation, C_v and C_I are given as:

$$\frac{dC_V}{dt} = (L+K) - R_{IV}(D_I + D_V)C_I C_V - S_V D_V C_V, \qquad (6)$$

$$\frac{dC_I}{dt} = K - R_{IV}(D_I + D_V)C_I C_V - S_I D_I C_I, \qquad (7)$$

when L = 0, eqs. (6) and (7) represent the same concentration variations under e^- irradiation. The time dependences of C_v and C_I during L+e^- irradiation are also shown in Fig. 3(a) for the convenient comparison with those during e^- irradiation. After laser irradiation the magnitude of sink strength was determined in the order of 10^{11}–10^{12} m^{-2} which is lower than the general value of e^- irradiation[16], thus lines in the colour of red and green represent dual-beam irradiation with $S = 2 \times 10^{11}$ m^{-2} and increasing point production rate under laser irradiation (L), respectively. C_v increases with L. Dual-beam irradiation has the similar stages with those of e^- irradiation. The recombination time of L+e^- irradiation is longer than that of e^- irradiation, which indicates SV and interstitial recombination is enhanced. Unlike e^- irradiation and L→e^- irradiation, SVs and FPs are introduced simultaneously during L+e^- irradiation. In the interior of the specimen, the interstitials and SVs co-exist nearby, as a result, their recombination is the dominant behaviour during L+e^- irradiation. Due to the higher C_v, void number density of

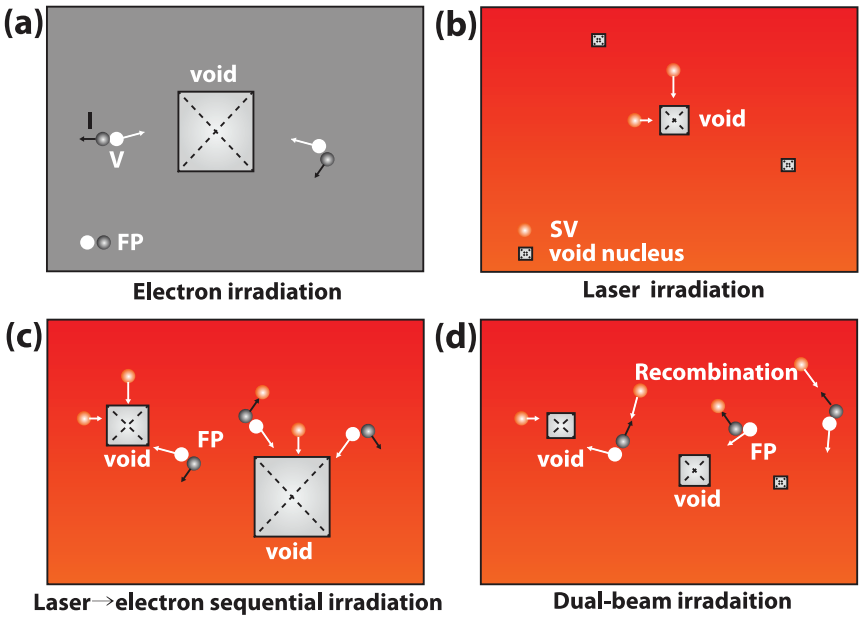

Figure 4 | Diagrams of the defect behaviours under different irradiation conditions. (a) Electron irradiation. FPs are introduced by electron irradiation; interstitials easily migrate to sinks, while vacancies gradually gather to form voids. (b) Laser irradiation. SVs are introduced at the surface of the specimen by laser irradiation, and subsequently diffuse to the interior and form into void nuclei, of which only a small number grow during the thermal annealing process. (c) Laser-electron sequential irradiations. Effect of pre-laser irradiation is the same as in Fig. 4(b), but subsequent electron irradiation perturbs the SVs, which leads to void nuclei growth. (d) Laser-electron dual-beam irradiation. SVs and FPs recombine because they are introduced simultaneously by laser irradiation and electron irradiation, respectively. Although void nucleation is abundant, growth is inhibited, and the void mean size is consequently smaller than that observed under any other conditions.

L+e^- irradiation is higher than that of e^- irradiation. But the void growth is delayed because of the delayed steady-state of L+e^- irradiation; therefore, the void size is much smaller than that of e^- irradiation and L→e^- irradiation, which causes the void swelling to decrease greatly. The details of all these calculations are given in the SI. Figure 4 (a), (b), (c) and (d) presents the models of how defect behaviour varies with the irradiation conditions.

In conclusion, SVs introduced by laser irradiation enhance void nucleation but contribute less to void growth. Subsequent electron irradiation perturbs the SVs, causing them to contribute to void growth and to thus increase swelling significantly. SV and interstitial recombination is greatly enhanced by L+e^- irradiation and acts as the dominant governing mechanism of the defect behaviour. Consequently, the degree of swelling due to L+e^- irradiation is less than that due to e^- irradiation or L→e^- irradiation. Therefore, L+e^- irradiation is shown to depress void swelling substantially in crystalline solids.

Methods

The chemical composition of the SUS316L austenite stainless steel used in this study is shown in Supplementary Table 1. The specimen preparation procedures and laser-HVEM operations were as previously described[16]. The irradiated area of specimen had a thickness of 300–550 nm.

Five different irradiation processes were performed using the laser-HVEM equipment to investigate the effect of laser irradiation on defect behaviour and void formation. The experimental procedures are given in Table 1. The central wavelength of the Nd: YAG laser was 532 nm with a repetition rate of 2 Hz, and pulse duration was 5–6 ns. The average energy density of the laser beam was measured at 24 mJ/cm^2. The laser beam energy used in this study to introduce defects inside the specimen was significantly lower than that of the laser-ion dual-beam irradiation process used for controlling nanoparticle precipitates at the surface of semiconductors[30]. Laser and electron irradiations were carried out at 723 K at which both interstitials and vacancies are thermally mobile. Due to the low diffusion rate of vacancies and the short laser irradiation time of 10 min (1200 laser pulses), thermal annealing for 90 min at 723 K was carried out following the single laser-beam irradiation, after which voids were expected to grow and subsequently be clearly visible. Electron irradiation was performed at 1000 kV, with a damage rate of 2×10^{-3} dpa/s, which is typical for electron irradiation. During the laser irradiation and thermal annealing steps, the electron beam intensity for transmission electron microscopy (TEM) observation was kept as low as possible to avoid any effects of this additional irradiation on the specimen. After irradiation, the voids were analysed using a JEM-2000ES TEM.

1. Adams, J. H. *Cosmic Ray Effects on Microelectronics, Part IV* (Washington, D.C., 1986).
2. Weir, J. R. Radiation damage at high temperatures. *Science* **156**, 1689 (1967).
3. Norris, D. I. R. Voids in nickel irradiated with electrons after previous argon ion bombardment. *Nature* **227**, 830–831 (1970).
4. Delarubia, T. D. & Gilmer, G. H. Structural transformations and defect production in Ion-implanted silicon - a molecular-dynamics simulation study. *Phys. Rev. Lett.* **74**, 2507–2510 (1995).
5. Seitz, F. Effects of irradiation on metals. *Science* **138**, 563–571 (1962).
6. Delarubia, T. D. Irradiation-induced defect production in elemental metals and semiconductors: a review of recent molecular dynamics studies. *Annu. Rev. Mater. Sci.* **26**, 613–649 (1996).
7. Cawthorn, C. & Fulton, E. J. Voids in irradiated stainless steel. *Nature* **216**, 575–576 (1967).
8. Masters, B. C. Dislocation loops in irradiated iron. *Philos. Mag.* **11**, 881–893 (1965).
9. Shewmon, P. G. Radiation-induced swelling of stainless steel. *Science* **173**, 987–991 (1971).
10. Lucas, G. E. The evolution of mechanical property change in irradiated austenitic stainless-steels. *J. Nucl. Mater.* **206**, 287–305 (1993).
11. Fraser, A. S., Birss, I. R. & Cawthorne, C. High-temperature embrittlement of stainless steel irradiated in fast fluxes. *Nature* **211**, 291–292 (1966).
12. Lewthwaite, G. W., Mosedale, D. & Ward, I. R. Irradiation creep in several metals and alloys at 100°C. *Nature* **216**, 472–473 (1967).
13. Byun, T. S., Farrell, K. & Li, M. K. Deformation in metals after low-temperature irradiation: Part II - Irradiation hardening, strain hardening, and stress ratios. *Acta Mater.* **56**, 1056–1064 (2008).
14. Kimoto, T., Allen, C. W. & Rehn, L. E. Growth-rate of dislocation loop in Fe-Ni-Cr alloy under Kr^+ ion and electron-irradiation. *J. Nucl. Mater.* **191**, 1194–1197 (1992).
15. Watanabe, S. *et al.* In situ observation of self-organizing nanodot formation under nanosecond-pulsed laser irradiation on Si surface. *J. Appl. Phys.* **108** 103510 (2010).
16. Yang, Z., Sakaguchi, N., Watanabe, S. & Kawai, M. Dislocation loop formation and growth under in-situ laser and/or electron irradiation. *Sci. Rep.* **1** 190 (2011).
17. Laidler, J. J. & Mastel, B. Nucleation of voids in irradiated stainless-steel. *Nature* **239**, 97–98 (1972).

18. Krishan, K. Kinetics of void-lattice formation in metals. *Nature* **287**, 420–421 (1980).
19. Hu, S. Y. & Henager, C. H. Phase-field simulation of void migration in a temperature gradient. *Acta Mater.* **58**, 3230–3237 (2010).
20. Maiman, T. H. Stimulated optical radiation in ruby. *Nature* **187**, 493–494 (1960).
21. Hendrick, D. A. & Meyers, A. Wound-healing after laser-surgery. *Otolaryng. Clin. N. Am.* **28**, 969–986 (1995).
22. Collis, R. T. H. & Ligda, M. G. H. Laser radar echoes from the clear atmosphere. *Nature* **203**, 508–508 (1964).
23. Cao, X., Jahazi, M., Immarigeon, J. P. & Wallace, W. A review of laser welding techniques for magnesium alloys. *J. Mater. Process. Technol.* **171**, 188–204 (2006).
24. Tian, Y. S., Chen, C. Z., Li, S. T. & Huo, Q. H. Research progress on laser surface modification of titanium alloys. *Appl. Surf. Sci.* **242**, 177–184 (2005).
25. Yoshida, Y., Sakaguchi, N., Watanabe, S. & Kato, T. Self-organized two-dimensional vidro-nanodot array on laser-irradiated Si surface. *Appl. Phys. Express* **4**, 055202 (2011).
26. Foreman, A. J. E. & Makin, M. J. Effect of vacancy loops on swelling of irradiated materials. *J. Nucl. Mater.* **79**, 43–57 (1979).
27. Delarubia, T. D. & Guinan, M. W. Progress in the development of a molecular-dynamics code for high-energy cascade studies. *J. Nucl. Mater.* **174**, 151–157 (1990).
28. Kiritani, M., Yoshida, N., Takata, H. & Maehara, Y. Growth of interstitial type dislocation loops and vacancy mobility in electron-irradiated metals. *J. Phys. Soc. Jpn.* **38**, 1677–1686 (1975).
29. Sizmann, R. Effect of radiation upon diffusion in metals. *J. Nucl. Mater.* **69–70**, 386–412 (1978).
30. Okubo, N., Umeda, N., Takeda, Y. & Kishimoto, N. Enhancement of metal-nanoparticle precipitation by co-irradiation of high-energy heavy ions and laser in silica glass. Nucl. *Instrum. Methods Phys. Res., Sect. B* **206**, 610–614 (2003).

Acknowledgements

The authors are grateful to Professors N. Sakaguchi, H. Takahashi, T. Shibayama and S. Yatsu for their helpful discussions on the present study. The authors are also grateful to Mr. K. Ohkubo for his help in operating the laser-HVEM system.

Author contribution

Z.B.Y. designed and performed the experiment, collected and analysed data and wrote the paper; S.W. designed the study, analysed data and assisted with writing the paper; T.K. was involved in the analysis. All authors discussed the results.

Additional information

Supplementary information accompanies this paper at http://www.nature.com/scientificreports

Competing financial interests: The authors declare no competing financial interests.

License: This work is licensed under a Creative Commons Attribution-NonCommercial-NoDerivativs 3.0 Unported License. To view a copy of this license, visit http://creativecommons.org/licenses/by-nc-nd/3.0/

How to cite this article: Yang, Z., Watanabe, S. & Kato, T. The Irradiation Effect of a Simultaneous Laser and Electron Dual-beam on Void Formation. *Sci. Rep.* **3**, 1201; DOI:10.1038/srep01201 (2013).